Preseismic TEC changes for Tohoku-Oki earthquake: Comparisons between simulations and observations

C. L. Kuo,[1] L. C. Lee,[1,2] and K. Heki[3]

[1] Institute of Space Science, National Central University, Jungli, Taiwan.
[2]Institute of Earth Sciences, Academia Sinica, Taipei, Taiwan.
[3]Department of Natural History Science, Hokkaido University, Japan

Abstract

Heki [2011] reported that the Japanese GPS dense network detected a precursory positive anomaly of total electron content (TEC), with ΔTEC ~ 3 TECU, ~40 minutes before the Tohoku-Oki earthquake (Mw9.0). Similar preseismic TEC anomalies were also observed in the 2010 Chile earthquake (Mw 8.8), 2004 Sumatra-Andaman (Mw 9.2) and the 1994 Hokkaido-Toho-Oki (Mw 8.3). In this paper, we apply our improved lithosphere-atmosphere-ionosphere coupling model to compute the TEC variations, and compare the simulation results with the reported TEC observations. For the simulations of Tohoku-Oki earthquake, we assume that the stressed associated current started ~ 40 minutes before the earthquake, linearly increased, and reached its maximum magnitude at the time of the earthquake main shock. It is suggested that a dynamo current density of ~25 nA m^{-2} is required to produce the observed ΔTEC ~ 3 TECU.

1. Introduction

The searching for earthquake precursors has been conducted for several decades. Scientists seek for seismo-related signatures in the atmosphere or ionosphere, and clarify possible signatures for precursor. Insufficiency in observational evidence drives more interdisciplinary investigations attempting to unveil possible clues related to earthquake activities. Several measurement methods, including VLF/LF electromagnetic wave anomalies [*Hayakawa et al.*, 2010; *Hayakawa et al.*, 2012], thermal anomaly [*Ouzounov and Freund*, 2004; *Ouzounov et al.*, 2006; *Pulinets and Ouzounov*, 2011], TEC (total electron content) variations [*Liu et al.*, 2000; *Liu et al.*, 2001; *Liu et al.*, 2004; *Zhao et al.*, 2008] were investigated. In particular, ionospheric TEC anomaly was one of the possible manifestations of seismo-ionosphere coupling process [*Pulinets and Boyarchuk*, 2004; *Pulinets and Ouzounov*, 2011]. *Zhao et al.* [2008] and *Liu et al.* [2009] reported that the TEC may have anomalously decreased or increased up to 5 - 20% several days before the 2008 Wenchuan earthquake (Mw7.9).

Recently, [*Heki*, 2011] found that ~40 minutes before the 2011 Tohoku-Oki earthquake (Mw9.0) the Japanese Global Positioning System (GPS) dense network GEONET detected clear precursory positive anomaly in TEC. Similar preseismic TEC anomalies were also observed in the 2010 Chile (Mw 8.8), 2004 Sumatra-Andaman (Mw 9.2) and the 1994 Hokkaido-Toho-Oki (Mw 8.3) earthquakes. The finding of TEC variations over the earthquake epicenter lacks physical mechanisms to explain these pre-earthquake ionospheric signatures.

Kuo et al. [2011, 2013] proposed an electric coupling model for the lithosphere-atmosphere-ionosphere (LAI) current system, as illustrated in **Figure 1**. The lithosphere dynamo in the earthquake preparation region drives the internal current ($\mathbf{J_d}$) downward, leading to the presence of a charge dipole. *Freund* [2010] has demonstrated that stressed rock can generate the currents and serves as a current dynamo in the lithosphere. Due to the finite conductivities in the lithosphere, atmosphere and ionosphere, the current flows downward from the ionosphere, through the atmosphere ($\mathbf{J}_1$) and the lithosphere, into the negative pole of the dynamo region. The current flowing out of the ionosphere will reduce the positive charges in the ionosphere which have a higher electric potential. The currents flowing in the atmosphere are obtained by directly solving the current continuity equation $\nabla \bullet \vec{J} = 0$ [*Kuo et al.*, 2013]. The current obtained in the atmosphere can be used to calculate the electric fields at the lower boundary of the ionosphere. These external electric fields are them imposed as the boundary condition for the SAMI3 ionosphere model. The $\mathbf{E}\times\mathbf{B}$ plasma motion leads to TEC variations in the ionosphere.

In the present study, we use this LAI coupling model to obtain the ionospheric TEC variations 40 minutes before the 2011 Tohoku-Oki earthquake. Our modeling results are then compared with the observed ionospheric precursor signatures (TEC variations).

2. The Japanese GEONET TEC observation for the 2011 Tohoku-Oki Earthquake

With the aid of the Japanese dense GPS observation network of GEONET (http://www.gsi.go.jp), a possible anomaly for earthquake precursor could be detected for the March 11, 2011, Tohoku-Oki earthquake (Mw9.0) [*Heki*, 2011; *Heki and Enomoto*, 2013]. *Heki* [2011] used GPS-TEC data to find a clear precursory positive anomaly of ionospheric TEC over the epicentral region. The TEC variations started ~40 minutes before the earthquake and reached nearly ten percent of the background TEC. At the time of the main shock (5:46UT), eight GPS satellites were visible there [*Heki*, 2011]. The coseismic ionospheric distrubances (CIDs) can be seen by the GPS satellites as the irregular TEC changes caused by acoustic waves ~10 minutes after the earthquake, and the ionospheric oscillations caused by the atmospheric waves or internal gravity waves 40~80 minutes after the earthquake.

Figure 2 shows the GPS trajectories of the sub-ionospheric points (SIP) assuming a thin layer at 300 km altitude. The near-by-passage of satellite 15 (red), 26 (green) and 27 (blue) are drawn as dots while the corresponding SIP are indicated by solid lines. Here we show the detailed GPS-TEC data associated with these GPS satellites; other GPS satellites have similar results. For Satellite 15, the time sequence of snapshots of the geographical distribution of TEC variations are shown in **Figure 3** from UT 05:06 to UT 06:00 with a time step of ~5 minutes. The Japanese GEONET has more than 1000, and the corresponding measured ΔTEC are shown in **Figures 3, 4 and 5** where each dot indicates the measured ΔTEC with color scale in units of TECU (1TECU = 10^{12} e/cm^2) in the bottom panel.

In **Figure 3**, near the northeast side of Japan close to the west side of the 2011 Tohoku-Oki earthquake epicenter, the positive anomaly of TEC is found to start at the time of 40 minutes before the earthquake (UT 05:46). The region with the increase of TEC grew in area and reached the maximum value of ΔTEC. The TEC variations dissipated and returned to normal after the CID caused by atmospheric waves generated by the earthquake main shock [*Calais and Minster*, 1995].

To confirm the TEC increases preceding the Earthquake, we also show the TEC measurement by Satellite 26 and 27 in **Figures 4 and 5**. The similar results of the increased TEC are found; for example the covered region observed by Satellite 26 is almost directly over the epicentral region. In the period from UT 05:46 to UT 05:51, the observed ΔTEC can reach its peak value ~ 5 TECU. At the time of UT 06:00, it is found that CID generated by earthquake main shock propagates outward, as shown in the dashed circle in **Figure 4**. The oscillatory variations of the ionosphere caused by atmospheric waves started at the time of ~10 minutes after the earthquake and lasted 40~80 minutes afterward [*Heki*, 2011; *Liu et al.*, 2011].

3. Simulation results from LAI coupling model

When subjected to stress, rocks can activate positive holes ($h^{\cdot}$) as charge carriers and generate electric currents [*Freund*, 2010]. The accumulation of positive hole charge carriers at the Earth surface and charged O_2^+ ions from field-ionization in the air near the region of stressed rock. As rocks are subjected to stress, rocks activate hole ($h^{\cdot}$)

charge carriers. With the exception of pure white marble, every igneous and high-grade metamorphic rock tested has produced hole $(h^{\bullet})$ charge carriers when stressed. The positive $(h^{\bullet})$ charge carriers can spread through any less stressed and even nominally unstressed rock. The unstressed rock becomes positively charged while the stressed rocks are negatively charged due to the loss of $(h^{\bullet})$ charge carriers in the stressed region. Even in oceanic region, e.g., the 2011 Tohoku-Oki earthquake in our case, charge carriers have higher mobility in the ocean than in the land because of its higher conductivity. The accumulated surface charge over land or ocean would drive the current outward. After the charge neutralization time, some surface charges are transported into the ionosphere. The equivalent effect is the current flowing into the ionosphere. The direction of dynamo current flowing in the atmosphere depends on the sign of the generated charges over Earth's surface near stressed rock region: downward to (upward from) negative (positive) surface charge regions.

Kuo et al. [2013] improved the coupling model of LAI system over the previous model [*Kuo et al.*, 2011] which is valid only for magnetic latitude 90° and underestimates the imposed electric field at the lower boundary of ionosphere. In the new model, we calculate currents in the atmosphere by directly solving the current continuity equation, $\nabla \cdot \mathbf{J} = 0$. The currents in the atmosphere can be solved for any arbitrary angle of magnetic field, i.e., any magnetic altitude. The dynamo current density required to generate the same amount of TEC variation is found to be smaller by a factor of ~30 compared to that obtained in our previous model. The typical value of dynamo current J_{max} used in the calculations is 10-100 nA m^{-2}, corresponding to ΔTEC of 1-7 TECU for the daytime ionosphere.

We use the electric coupling model [*Kuo et al.*, 2011; *Kuo et al.*, 2013] to study the TEC increases before the 2011 Tohoku-Oki Earthquake [*Heki*, 2011]. The simulation results in our coupling models are compared with the observed TEC from GEONET. The parameters in the atmosphere-ionosphere coupling model are listed below. The details in the atmospheric current model and the ionosphere model are described in Section 3, respectively.

3.1. The atmospheric current model

Our assumed atmospheric current model:

- Fault region: 450 km in length and 200 km in width [Heki, 2011], azimuth angle ~30 degree from North

- Shift 1.5° west in longitude for EQ epicenter (38.3N,142.4E) toward the land
- Maximum current density J_{max} = 25 nA m^{-2}
- Current density linearly increasing from zero to its maximum value in the 40 minute period (UT 05:06-05:46) before the main shock

In our atmospheric current model, we assume current distribution near the ground surface, which is confined to a region with the length 2*a* and the width 2*b*.

$$J_{surf}(x,y) = \frac{-J_{\max}}{4}\left[1+\cos\frac{\pi(x-x_0)}{a}\right]\left[1+\cos\frac{\pi(y-y_0)}{b}\right] \tag{1}$$

for $x_0 - a < x < x_0 + a$ and $y_0 - b < y < y_0 + b$, where the center (x_0, y_0) of charge region is located near the epicenter. The negative sign in above equation indicates the current flowing downward. The maximum current density J_{max} is 25 nA m^{-2}, and the total current can be integrated as $I = a \times b \times J_{max}$. We assume a generated current source region with *a* = 200 km and *b* = 450 km, which is about the size of the fault region for the Tohoku-Oki earthquake.

The current system in the atmosphere is numerically solved using $\nabla \cdot \mathbf{J} = 0$ in 3D Cartesian coordinates (*x, y, z*) where the *x*–axis is east-west, the *y*–axis is north-south, -1000 ≤ *x*, *y* ≤ 1000 km, and the *z*-axis is the altitude, 0 ≤ *z* ≤ 200 km. The upper ionospheric boundary condition is $\frac{\partial J_z}{\partial z} = 0$. **Figure 6** shows an example of dynamo current with J_{max} = 25 nA m^{-2}, *a* = 200 km and *b* = 450 km: **Figure 6a** for the current density in the *y* = 0 plane, and **6b** for that in the *x* = 0 plane, and the white lines indicate the current flows. The peak current density at altitude z = 85 km is about -12.5 nA m^{-2}.

The nearly upward or downward current **J** flowing at 85 km altitude generally makes an angle with the inclined magnetic field. The imposed electric field on the lower boundary of the ionosphere can be derived by $E = \overleftrightarrow{\sigma}^{-1} J$ where conductivity tensor $\overleftrightarrow{\sigma}$ is expressed by [*Park and Dejnakarintra*, 1973],

$$\overleftrightarrow{\sigma} = \begin{pmatrix} \sigma_1 & \sigma_2 \sin\theta_b & \sigma_2 \cos\theta_b \\ -\sigma_2 \sin\theta_b & \sigma_1 \sin^2\theta_b + \sigma_0 \cos^2\theta_b & (\sigma_1 - \sigma_0)\sin\theta_b \cos\theta_b \\ -\sigma_2 \cos\theta_b & (\sigma_1 - \sigma_0)\sin\theta_b \cos\theta_b & \sigma_1 \cos^2\theta_b + \sigma_0 \sin^2\theta_b \end{pmatrix}, \tag{2}$$

where σ_0, σ_1 and σ_2 are the conductivity along the magnetic field, Pedersen conductivity and Hall conductivity, respectively; θ_b is the inclined angle of the magnetic field line and the horizontal plane. The values of the elements of $\overleftrightarrow{\sigma}$ are adopted from ionosphere model SAMI3 (see below). **Figure 6c** shows the imposed electric field on the upper (lower) boundary of the atmosphere (ionosphere) for the current distribution in **Figures 6a and 6b**.

The imposed electric field at the lower boundary of ionosphere can be used to study the TEC variations. The conductivity along the magnetic field-of-line in the ionosphere is very high. The potential along the field-of-line is nearly equal potential. The imposed electric field can change the electric field potential along the field-of-line in the ionosphere. Therefore, we impose the electric field caused by the upward current from the lower atmosphere, which is served as the electric disturbance source in the ionosphere.

3.2. The ionosphere model coupling with atmospheric current system

The parameters in the ionosphere model (SAMI3) are:

- Day 70 (Mar 11) in 2011
- Solar photoionization in the ionosphere (TEC)
  F10.7 index =150, and F10.7A=150 (81-day average of the daily F10.7)
- Geomagnetic Disturbance Index
  AP =4 (mild geomagnetic condition)
- Neutral wind model: HWM07
- Simulation region +/- 8° in longitude, grid size (*nf*, *nz*, *nl*)=(240,101,70)

The NRL three-dimensional ionosphere simulation code SAMI3 (http://wwwppd.nrl.navy.mil/sami2-OSP/index.html), including ion dynamics and electric potential, is used to investigate the TEC variation caused by the electric field from the source charge of earthquake fault zone. We solve the current continuity equation ($\nabla \cdot \mathbf{J} = 0$) in the ionosphere [*Huba et al.*, 2008; *Huba et al.*, 2009a; *Huba et al.*, 2009b; *Huba et al.*, 2009c], and obtain the electric potential in the ionosphere model SAMI3. The resulting electric field is used to study the plasma motion in the ionosphere caused by the source charge of the earthquake fault zone.

4. Comparisons between modeling results and the observation

The 2011 Tohoku-Oki earthquake had a fault region of ~450 km in length and ~200 km in width along the Japan Trench where the Packfic Plate subducts beneath NE Japan, as modeled above [*Heki*, 2011]. The orientation of the fault region has an azimuth angle ~30 degree from north centered at epicenter (38.3N, 142.4E). It is assumed that the maximum current density J_{max} = 25 nA m^{-2} increases linearly from zero to its maximum value in the 40 minute period (UT 05:06-05:46) before the main shock, as shown in **Figure 7**, since the increase of TEC is found to start at the time of 40 minutes before the earthquake (UT 05:46), and the region with the increase of TEC grew in area and reached the maximum of ΔTEC.

4.1. Simulation results of currents from the atmosphere

In comparison with the simulation results of *Kuo et al.* [2013], the modeling results show the presence of the eastward (westward) electric field for downward (upward) dynamo current flowing from the atmosphere into the ionosphere. At magnetic latitude 30°, close to the epicenter, the imposed eastward (westward) electric field causes the nearly upward-northward or downward-southward direction of **E**×**B** motion for ionospheric plasma, shown in **Figure 8a**. For the nearly upward-northward direction of plasma motion with eastward electric field caused by the downward current, the **E**×**B** motion drives the ionospheric plasma from the higher density region to the lower density region, enhancing the plasma density (**Figure 8c)** and increasing the TEC (**Figure 8b**). Hence, we choose the downward current with eastward electric field as our dynamo current.

The typical value of dynamo current J_{max} used in the calculations is 10-100 nA m^{-2}, corresponding to ΔTEC up to 1-7 TECU in the daytime case, shown in **Figure 9.** It is also found that, in the nighttime case, the smaller value of dynamo current (1-10 nA m^{-2}) can lead to similar ΔTEC values. In our calculation, the dynamo current equals to the multiplication of ionospheric conductivity and caused electric field. The typical daytime ionospheric conductivity is ten times of the nighttime conductivity. Therefore, the greater current density are required to reach the equivalent ΔTEC for the daytime ionosphere.

4.2. Observation results in comparison with simulation results

Figures 10a -10c show the observed TEC variations at SIP of more than 1000 ground GPS sites in the Japanese GEONET and their corresponding ΔTEC measurements are indicated by the color dots in units of TECU. **Figures 10d-10f** show the TEC contour lines from the simulation. **Figures 10e-10i** show the filled color contours of TEC where the color code indicates the value of TECU. The applied eastward electric field leads to the upward **E**×**B** motion and the increase of TEC. The ΔTEC shown in **Figures 10g, 10h and 10i** can be used to compare with measured ΔTEC results in **Figures 10a, 10b and 10c**.

Figure 11 shows the comparison of ΔTEC profiles from modeling results (red dots) with observation (blue dots) in units of TECU one minute before the time of main shock. **Figure 11a** is for the profile at geolontitude 139°, 11b at 140° and 11c at 141°. **Figures 11d, 11e and 11f** are for the profiles at geolatitude 36°, 38° and 40°. The modeling results with $J_{max} \approx 25$ nA m^{-2} are approximately matched with observations results.

5. Summary and discussions

Heki [2011] reported that ~ 40 minutes before the 2011 Tohoku-Oki earthquake the Japanese GPS dense network detected clear earthquake precursor signals of positive TEC variations over the epicentral region. We use the LAI coupling model to reproduce the observed ΔTEC 40 minutes before 2011 earthquake. We assume the area of dynamo current is similar to the earthquake fault region with a length $2a$ and a width $2b$ where a = 200 km and b = 450 km. It is found that the required dynamo current with the magnitude of 10-100 nA m^{-2} can produce ΔTEC of 1-7 TECU. In order to explain the observed ΔTEC ~ 3 TECU by *Heki* [2011; 2013], the dynamo current with $J_{max} = 25$ nA m^{-2} is required.

There are several areas for improvement and for future study. First, in our study, we have to assume a dynamo current source. More work on the dynamo source in the Earth's lithosphere is needed. The assumed dynamo current source under the ground is only based on the experimental evidence of stressed rocks by *Freund* [2010] and references therein.

Second, it is assumed in the SAMI3 ionosphere model that conductivity along the magnetic field is infinite and the associated electric field along the magnetic field is zero. In real ionosphere, we should consider the finite conductivity along the magnetic field. The currents from the earthquake region flow into the ionosphere. Part of the currents flow along the magnetic field, reflect from the ionosphere of the opposite hemisphere, and return to the current injection region. Although our simulation results show the conjugate effect, such as plasma and temperature variations, in the opposite hemisphere as shown in **Figure 8**, the conjugate effect may be decreased due to a finite field-aligned conductivity.

Third, it is suggested to carry out simultaneous measurements of the dynamo current and electric field under the ground, the current and electric field above the Earth's surface, and ionosphere TEC from ground GPS sites. The coordinated observations will help to resolve the linkage among the dynamo current in the lithosphere, currents in the atmosphere, and TEC variations in the ionosphere.

Acknowledgements

We acknowledge the discussion with. Ben Chao, Li Zhao, Tiger Liu, Cheng-Horng Lin and Chieh-Hung Chen. We are grateful to the National Center for High-performance Computing in Taiwan and Center for Computational Geophysics in the National Central University for computing suppoerts. This work is supported in part by grants (NSC 101-2628-M-001-007-MY3, NSC 102-2119-M-001 -014, and NSC 102-2111-M-008 -016) from the National Science Council of Taiwan.

References

Calais, E., and J. B. Minster (1995), GPS detection of ionospheric perturbations following the January 17, 1994, Northridge Earthquake, *Geophys. Res. Lett.*, *22*(9), 1045-1048, doi:10.1029/95gl00168.

Freund, F. (2010), Toward a unified solid state theory for pre-earthquake signals, *Acta Geophysica*, *58*(5), 719-766, doi:10.2478/s11600-009-0066-x.

Hayakawa, M., Y. Kasahara, T. Endoh, Y. Hobara, and S. Asai (2012), The observation of Doppler shifts of subionospheric LF signal in possible association with earthquakes, *J. Geophys. Res. Space Physics*, *117*(A9), A09304, doi:10.1029/2012ja017752.

Hayakawa, M., Y. Kasahara, T. Nakamura, F. Muto, T. Horie, S. Maekawa, Y. Hobara, A. A. Rozhnoi, M. Solovieva, and O. A. Molchanov (2010), A statistical study on the correlation between lower ionospheric perturbations as seen by subionospheric VLF/LF propagation and earthquakes, *J. Geophys. Res. Space Physics*, *115*(A9), A09305, doi:10.1029/2009ja015143.

Heki, K. (2011), Ionospheric electron enhancement preceding the 2011 Tohoku-Oki earthquake, *Geophys. Res. Lett.*, *38*(17), L17312, doi:10.1029/2011gl047908.

Heki, K., and Y. Enomoto (2013), Preseismic ionospheric electron enhancements revisited, *J. Geophys. Res. Space Physics*, 118, 6618–6626, doi:10.1002/jgra.50578.

Huba, J. D., G. Joyce, and J. Krall (2008), Three-dimensional equatorial spread F modeling, *Geophys. Res. Lett.*, *35*, 10102, doi:10.1029/2008GL033509.

Huba, J. D., J. Krall, and G. Joyce (2009a), Atomic and molecular ion dynamics during equatorial spread F, *Geophys. Res. Lett.*, *36*, 10106, doi: 10.1029/2009GL037675.

Huba, J. D., G. Joyce, J. Krall, and J. Fedder (2009b), Ion and electron temperature evolution during equatorial spread F, *Geophys. Res. Lett.*, *36*, 15102, doi:10.1029/2009GL038872.

Huba, J. D., S. L. Ossakow, G. Joyce, J. Krall, and S. L. England (2009c), Three-dimensional equatorial spread F modeling: Zonal neutral wind effects, *Geophys. Res. Lett.*, *36*, 19106, doi:10.1029/2009GL040284.

Kuo, C. L., L. C. Lee, and J. D. Huba (2013), An improved coupling model for the lithosphere-atmosphere-ionosphere system, *J. Geophys. Res. Space Physics*, revised.

Kuo, C. L., J. D. Huba, G. Joyce, and L. C. Lee (2011), Ionosphere plasma bubbles and density variations induced by pre-earthquake rock currents and associated surface charges, *J. Geophys. Res. Space Physics*, *116*(A10), A10317, doi:10.1029/2011ja016628.

Liu, J. Y., Y. I. Chen, Y. J. Chuo, and H. F. Tsai (2001), Variations of ionospheric total electron content during the Chi-Chi earthquake, *Geophys. Res. Lett.*, *28*, 1383-1386, doi:10.1029/2000GL012511.

Liu, J. Y., Y. I. Chen, S. A. Pulinets, Y. B. Tsai, and Y. J. Chuo (2000), Seismo-ionospheric signatures prior to M>=6.0 Taiwan earthquakes, *Geophys. Res. Lett.*, *27*, 3113-3116, doi:10.1029/2000GL011395.

Liu, J. Y., Y. Chuo, S. Shan, Y. Tsai, Y. Chen, S. Pulinets, and S. Yu (2004), Pre-earthquake ionospheric anomalies registered by continuous GPS TEC measurements, *Ann. Geophys.*, *22*(5), 1585-1593, doi:10.5194/angeo-22-1585-2004.

Liu, J. Y., et al. (2009), Seismoionospheric GPS total electron content anomalies observed before the 12 May 2008 M_w7.9 Wenchuan earthquake, *J. Geophys. Res. Space Physics*, *114*, 04320, doi:10.1029/2008JA013698.

Liu, J. Y., C. H. Chen, C. H. Lin, H. F. Tsai, C. H. Chen, and M. Kamogawa (2011), Ionospheric disturbances triggered by the 11 March 2011 M9.0 Tohoku Earthquake, *J. Geophys. Res.*, *116*, A06319, doi:10.1029/2011JA016761.

Ouzounov, D., and F. Freund (2004), Mid-infrared emission prior to strong earthquakes analyzed by remote sensing data, *Adv. Space Res.*, *33*(3), 268-273, doi:10.1016/S0273-1177(03)00486-1.

Ouzounov, D., N. Bryant, T. Logan, S. Pulinets, and P. Taylor (2006), Satellite thermal IR phenomena associated with some of the major earthquakes in 1999–2003, *Physics and Chemistry of the Earth, Parts A/B/C*, *31*(4–9), 154-163, doi:10.1016/j.pce.2006.02.036.

Park, C. G., and M. Dejnakarintra (1973), Penetration of Thundercloud Electric Fields into the Ionosphere and Magnetosphere, 1. Middle and Subauroral Latitudes, *J. Geophys. Res.*, *78*(28), 6623-6633, doi:10.1029/JA078i028p06623.

Pulinets, S., and K. Boyarchuk (2004), *Ionospheric precursors of earthquakes*, 315 p.p. pp., Springer, Berlin.

Pulinets, S., and D. Ouzounov (2011), Lithosphere–Atmosphere–Ionosphere Coupling (LAIC) model – An unified concept for earthquake precursors validation, *J. Southeast Asian Earth Sci.*, *41*(4–5), 371-382, doi:10.1016/j.jseaes.2010.03.005.

Zhao, B., M. Wang, T. Yu, W. Wan, J. Lei, L. Liu, and B. Ning (2008), Is an unusual large enhancement of ionospheric electron density linked with the 2008 great Wenchuan earthquake?, *J. Geophys. Res. Space Physics*, *113*, 11304, doi:10.1029/2008JA013613.

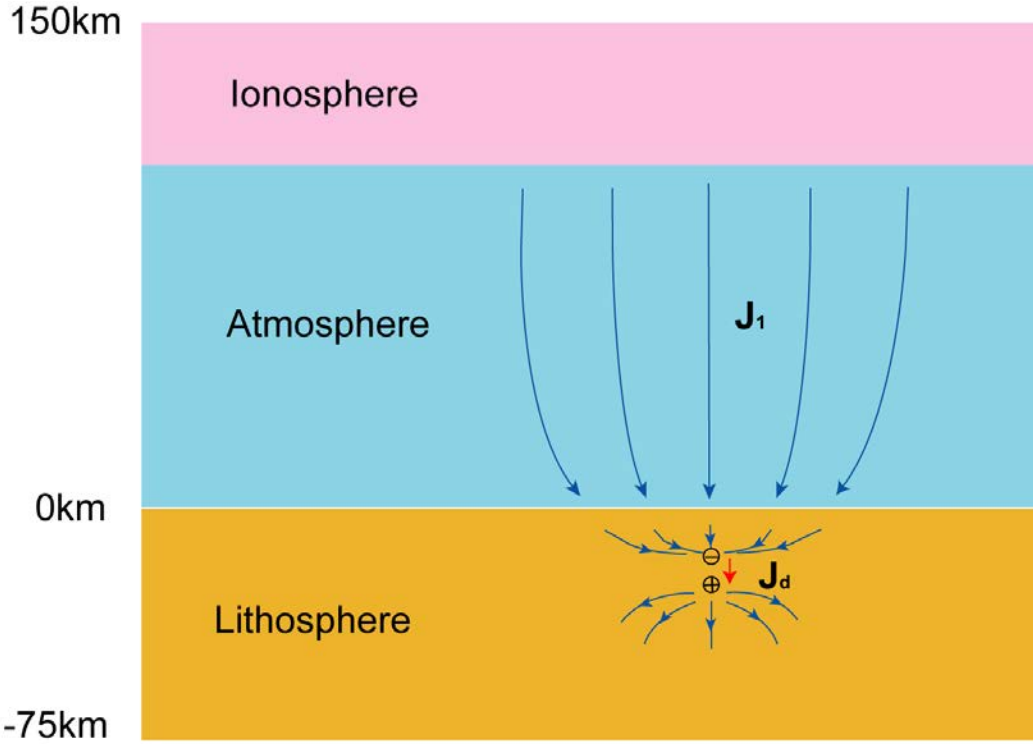

Figure 1. The current flow in the electric coupling model of lithosphere, atmosphere and ionosphere. The lithosphere dynamo has a charge dipole generated by the internal current $\mathbf{J}_d$. The current flows downward from the ionosphere, through the atmosphere ($\mathbf{J}_1$) and lithosphere, into the negative pole of the dynamo region.

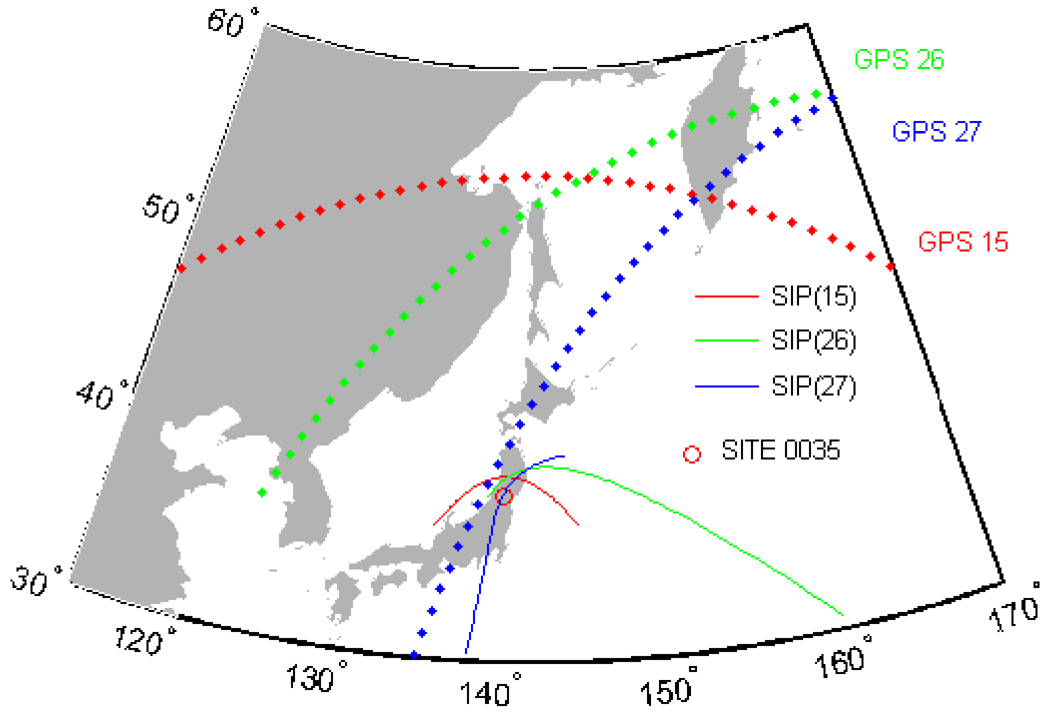

Figure 2. The trajectories of sub-ionospheric points (SIP) assuming a thin layer at 300 km altitude for GPS satellites and given ground GPS site 0035. The near-by-passage of satellite 15, 26 and 27 are drawn as dots while the corresponding SIPs for GPS 15, 26 and 27 are indicated by solid lines. Within the dots and solid lines, the GPS satellite 15, 26 and 27 are colorized as red, green and blue lines.

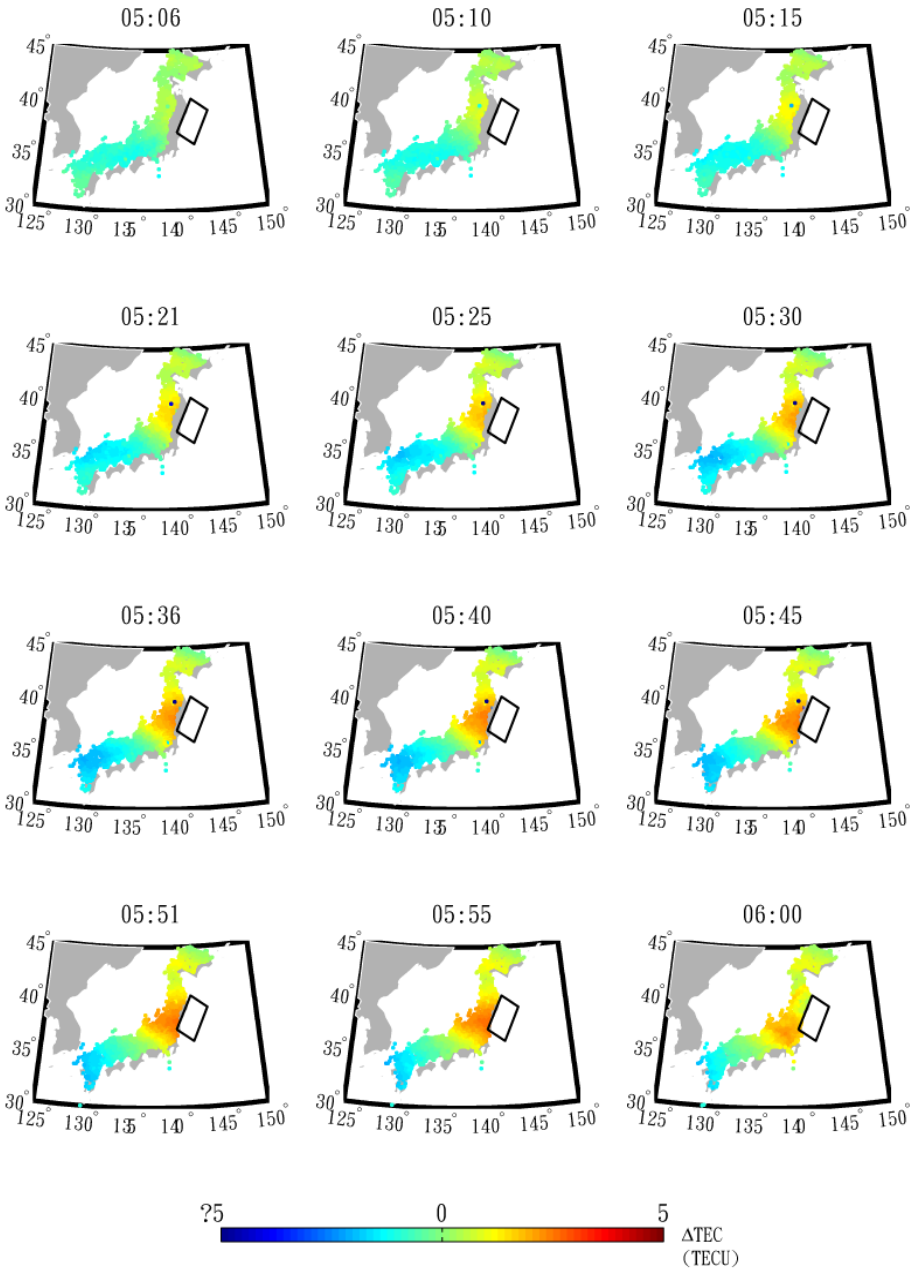

Figure 3. The time sequence of ΔTEC recorded by the GPS satellite 15 with a time step of 5 minutes at a period 40 minutes before and 15 minutes after the 2011 Tohoku-Oki Earthquake (UT 05:46). The rectangular with black lines indicates the fault region of earthquake (~450 km in length and ~ 200 km in width along the Japan). The color code indicates the increase (red color) of TEC or the decrease (blue color) of TEC where the unit of TEC is TECU (1TECU = 10^{12} e/cm^2).

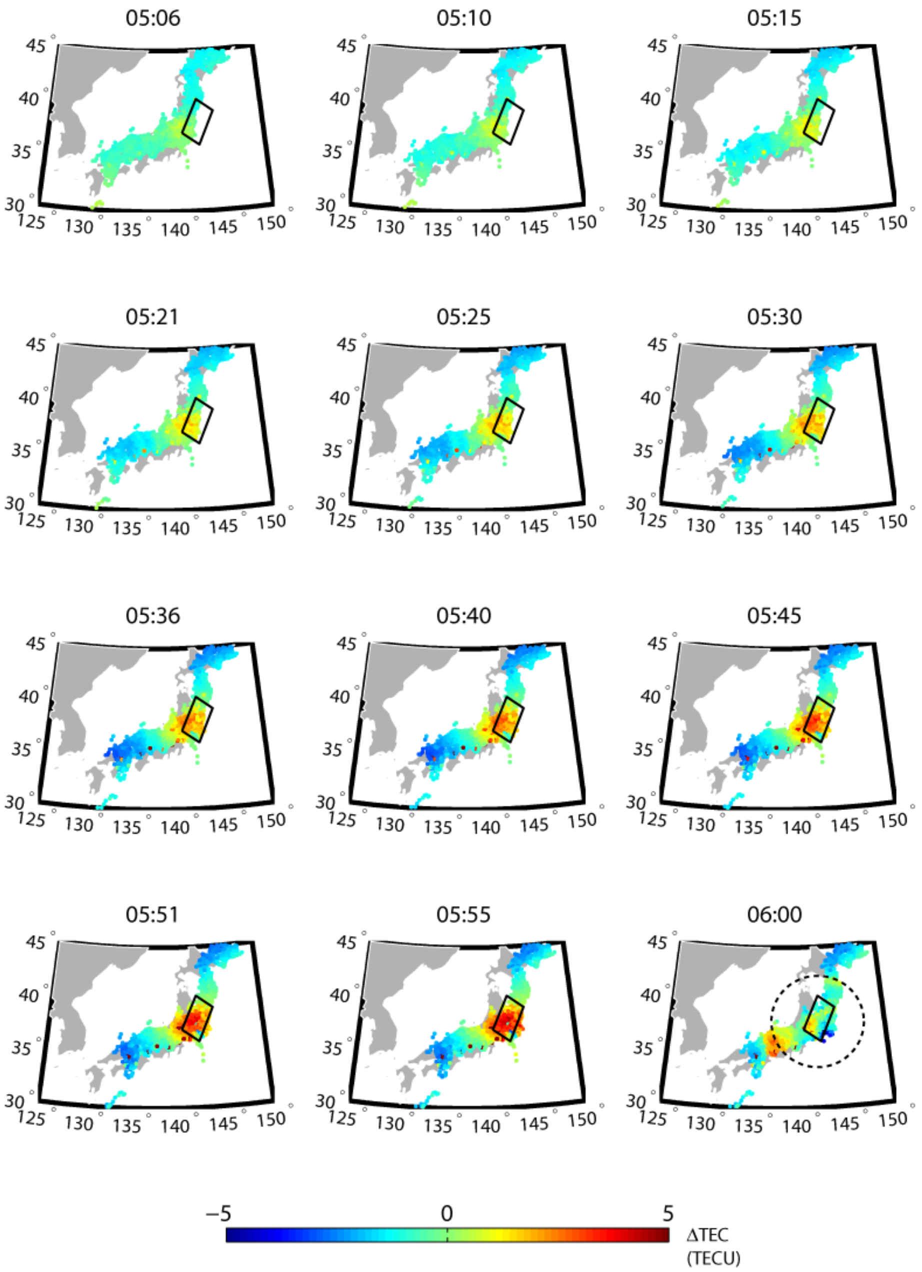

Figure 4. The time sequence of ΔTEC recorded by the GPS satellite 26 with a time step of 5 minutes at a period 40 minutes before and 15 minutes after the 2011 Tohoku-Oki Earthquake (UT 05:46). In the right and bottom panel, a dashed circle indicates the CID generated by earthquake propagating outwardly after the main shock.

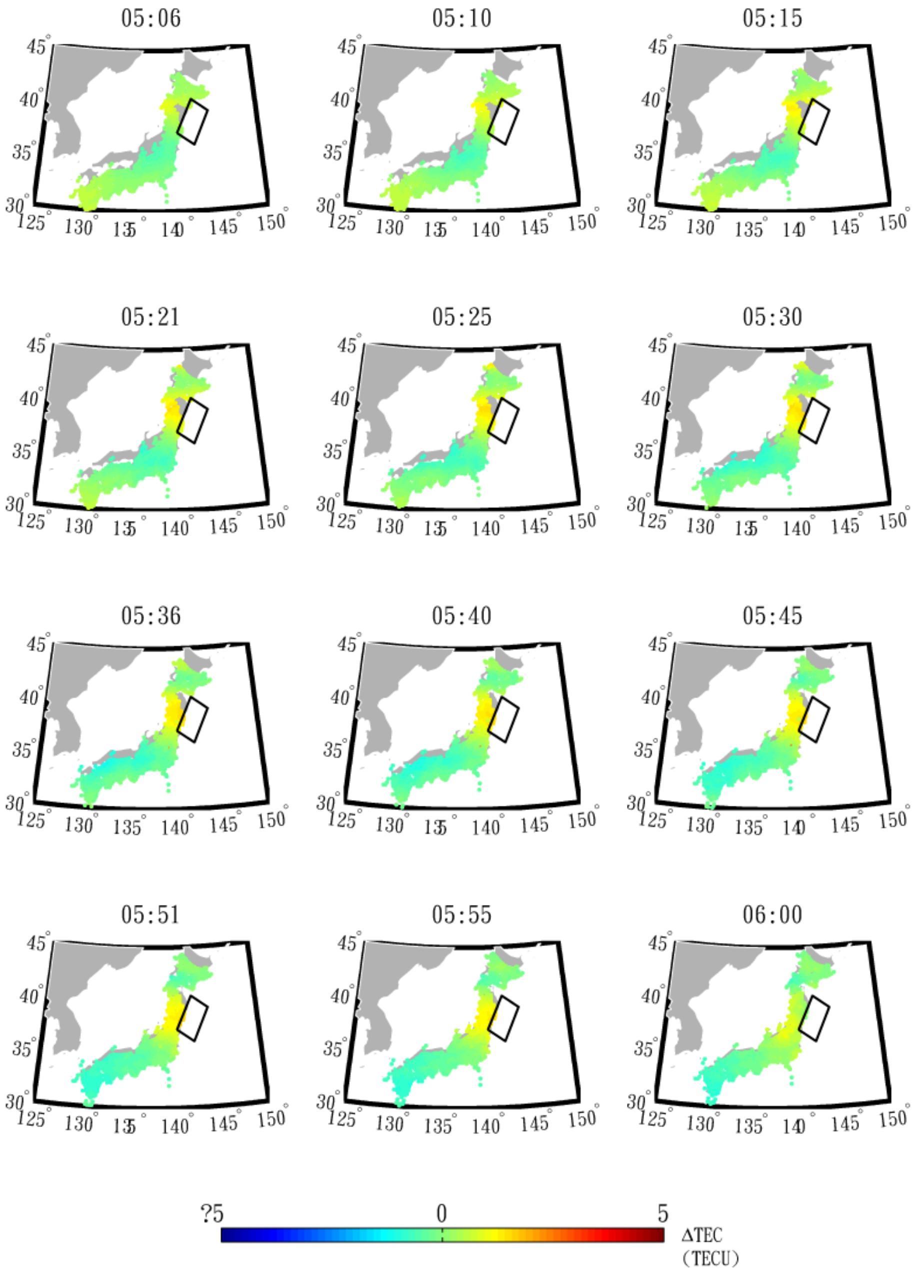

Figure 5. The time sequence of ΔTEC recorded by the GPS satellite 27 with a time step of 5 minutes at a period 40 minutes before and 15 minutes after the 2011 Tohoku-Oki Earthquake (UT 05:46).

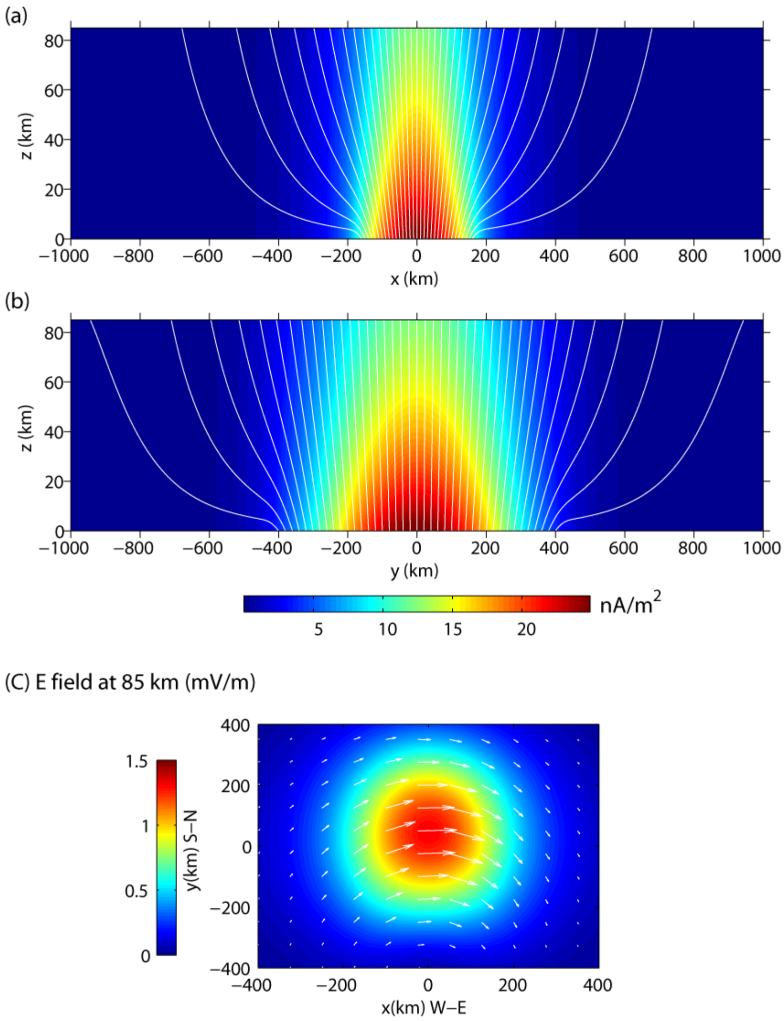

Figure 6. The distribution of current densities in (a) the $y = 0$ plane and (b) the $x = 0$ plane of the atmosphere. The current density is expressed in colors and the white lines are current flow lines. (c) The eastward electric field at an altitude of 85 km.

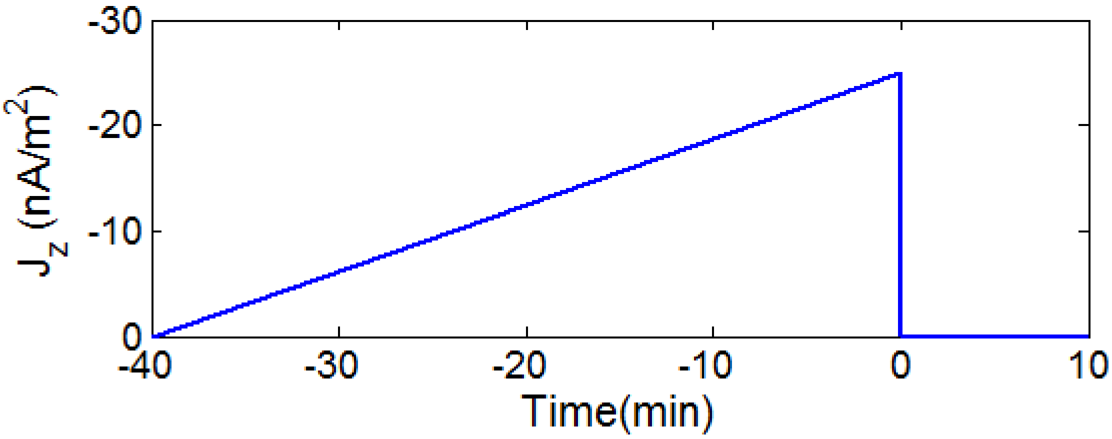

Figure 7. The maximum current density linearly increases from zero to its maximum value in the 40 minute period (UT 05:06-05:46) before the main shock.

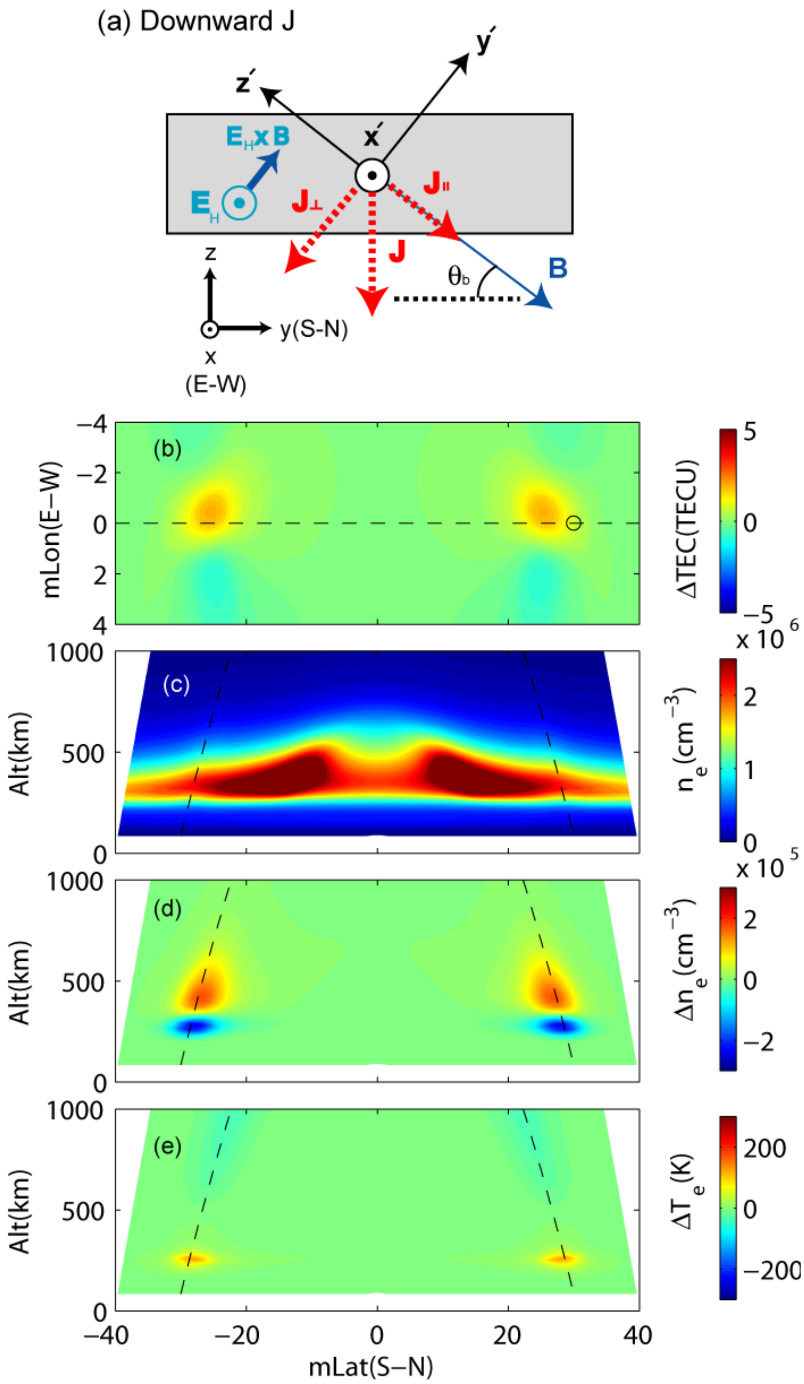

Figure 8. The ionospheric anomaly caused by downward current at the magnetic latitude 30°; (a) the downward current lead to the presence of eastward electric field and the caused **E**×**B** motion enhance the ionospheric plasma density; (b) contour plots of ΔTEC in units of TECU where open circle indicate the source region; (c) contour plots of electron density n_e in the meridional planes; (d) contour plots of electron density variations Δn_e in the meridional planes; (e) temperature variations in the meridional planes.

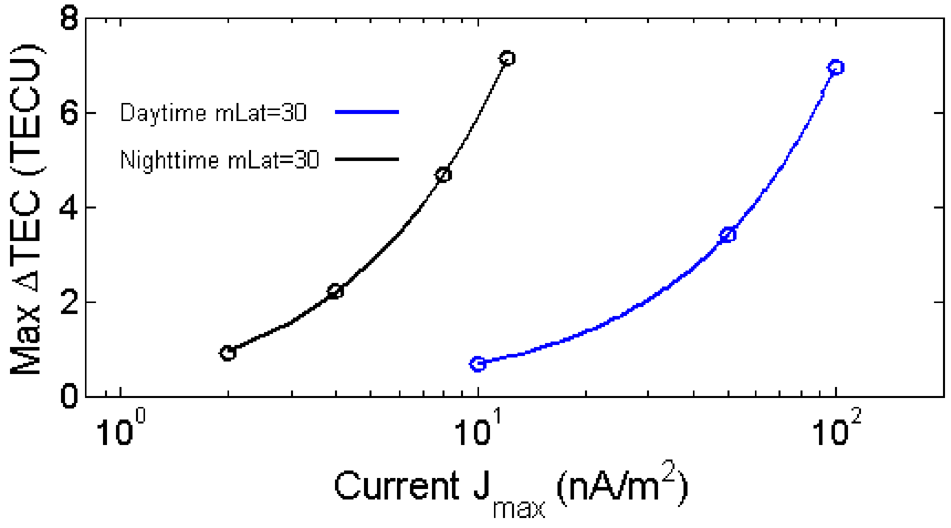

Figure 9. The maximum ΔTEC (TECU) varies with source current density $J_{\max}$ in units of nA m^{-2} where the solid (dashed) lines are for ΔTEC at magnetic latitude 30°. The blue (black) lines are for daytime (nighttime) ionosphere.

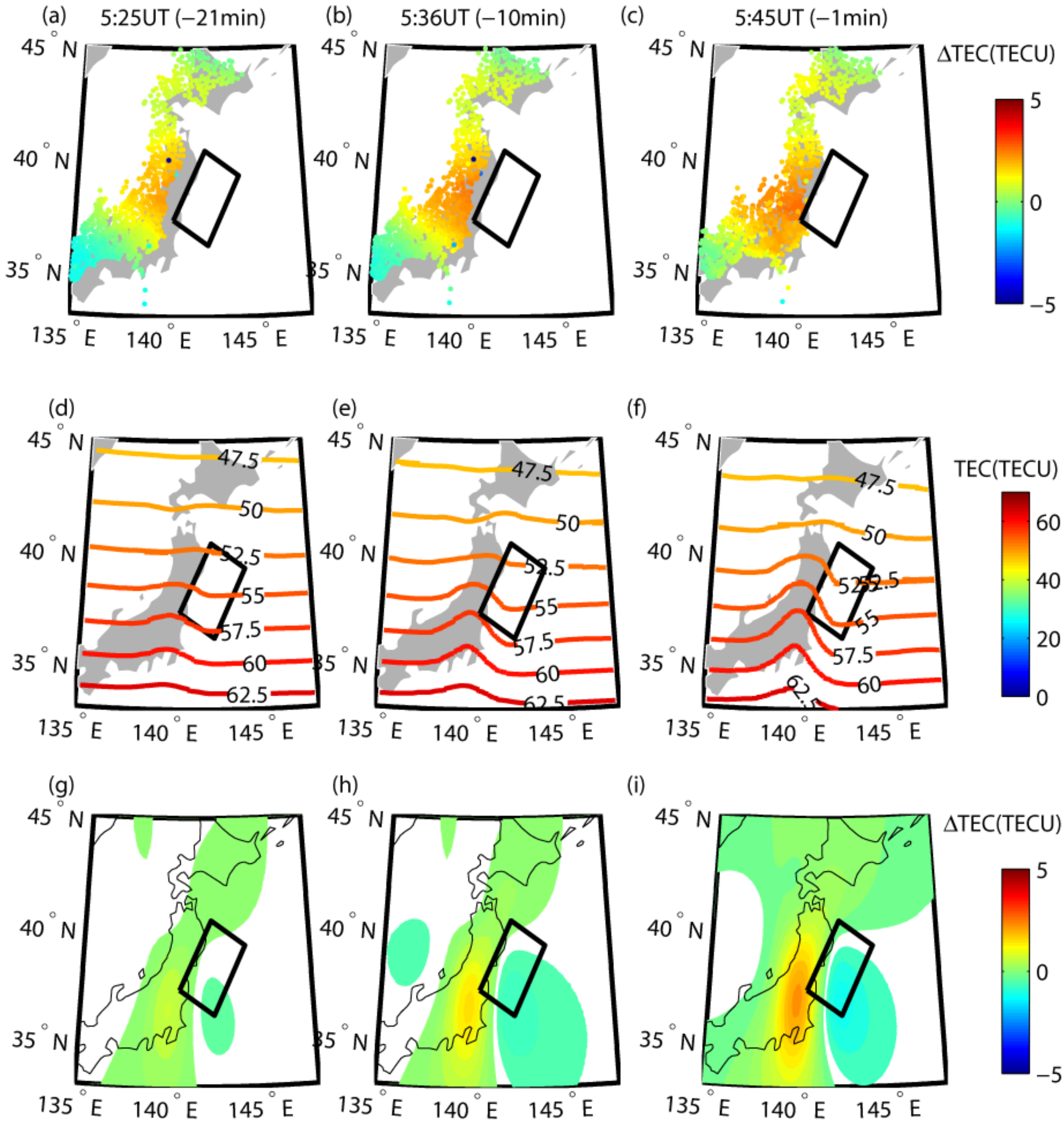

Figure 10. The observed results of ΔTEC from the Japanese GEONET where color code indicates the magnitude of TEC in a time sequence of (a) 21 minutes, (b) 10 minutes and (c) 1 minute before the main shock of the earthquake. The corresponding TEC contour lines from our simulation results are plotted in (d), (e) and (f). The corresponding ΔTEC from our simulation results are plotted in (g), (h) and (i).

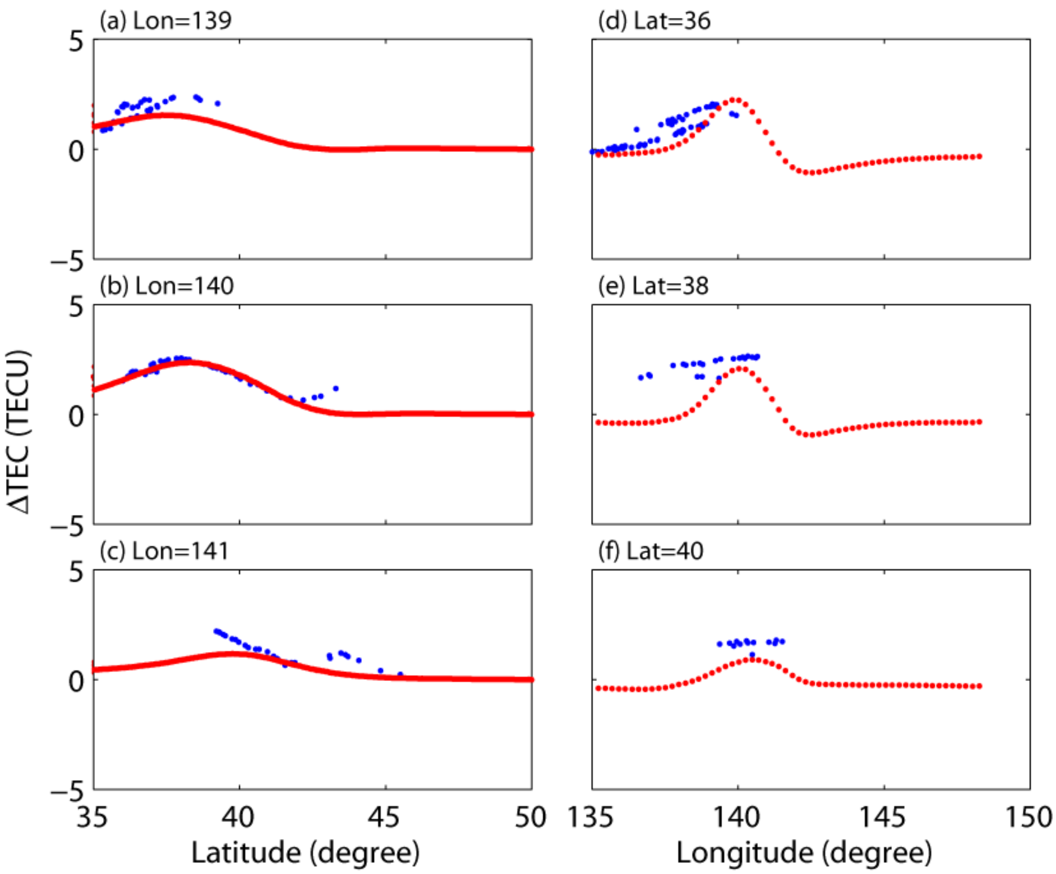

Figure 11. The comparison of modeling results (red dots) with observed ΔTEC (blue dots) in units of TECU at UT 05:45, one minute before the time of main shock: (a) the profile at geolontitude 139°, (b) the profile at geolontitude 140°, (c) the profile at geolontitude 141°, (d) the profile at geolatitude 36°, (e) the profile at geolatitude 38°, and (f) the profile at geolatitude 40°.